# Effect of neutrino electromagnetic form factors on the neutrino cross section in dense matter

A. Sulaksono, C. K. Williams, P. T. P. Hutauruk, and T. Mart
*Departemen Fisika, FMIPA, Universitas Indonesia, Depok, 16424, Indonesia*
(Received 5 September 2005; published 13 February 2006)

The sensitivity of the differential cross section of the interaction between a neutrino-electron and dense matter to the possibly nonzero neutrino electromagnetic properties has been investigated. Here, the relativistic mean field model inspired by effective field theory has been used to describe nonstrange dense matter, both with and without the neutrino trapping. We have found that the cross section becomes more sensitive to the constituent distribution of the matter, once electromagnetic properties of the neutrino are taken into account. The effects of neutrino electromagnetic properties on the cross section become more significant for the neutrino magnetic moment $\mu_\nu > 10^{-10}\mu_B$ and for the neutrino charge radius $R > 10^{-5}\,\mathrm{MeV}^{-1}$.

DOI: 10.1103/PhysRevC.73.025803 PACS number(s): 13.15.+g, 25.30.Pt, 97.60.Jd

## I. INTRODUCTION

The demand for precise information on neutrino transport in the investigations of astrophysical phenomena, such as supernovae explosion and the structure of protoneutron stars, has stimulated several studies on neutrino interactions in matter at high densities [1–14]. Even recently, a realistic neutrino opacity in neutron-rich matter for the supernovae simulation which takes into account the correlations and weak magnetism of nucleons in the finite temperature calculations has been also considered [4].

In the standard model, massless neutrinos have zero magnetic moment and electronic charge. However, there is evidence that the laboratory bound on the neutrino-electron magnetic moment ($\mu_\nu$) is smaller than $1.0 \times 10^{-10}\mu_B$ at the 90% confidence level [15], where $\mu_B$ is the Bohr magneton. A stronger bound of $\mu_\nu \leqslant 3.0 \times 10^{-12}\mu_B$ also exists from astrophysical consideration, particularly from the study of the red giant population in the globular cluster [16]. On the other hand, the charge radius of $\nu_e$ has been bounded by the Los Alamos Meson Facility (LAMF) experiment [17] to be $R^2 = (0.9 \pm 2.7) \times 10^{-32}\,\mathrm{cm}^2 = (22.5 \pm 67.5) \times 10^{-12}\,\mathrm{MeV}^{-2}$, while the plasmon decay in the globular cluster star predicts the limit of $e_\nu \leqslant 2 \times 10^{-14}\,e$ [16], where $e$ is electron charge. Recent discussions on the effects of the neutrino electromagnetic properties in astrophysics can be seen in, e.g., Ref. [16]; for the case of the solar neutrino problem, one can consult, e.g., Ref. [18].

So far, there has been no calculation of the interaction of neutrinos with dense matter which considers neutrino electromagnetic form factors. To this end, we extend our previous report of the interaction of neutrinos with electron gas [14] to the interaction of neutrinos with the nonstrange dense stellar matter, taking into account the effects of the trapped neutrinos in matter, but still using the zero temperature approximation. The validity of this approximation is fulfilled by the fact that temperature effects on the equation of state (EOS) of supernovae matter and maximum masses of protoneutron stars are smaller than those without neutrino trapping [19]. We note that considerable effort has been devoted to studying the effective electromagnetic coupling of neutrinos in the thermal background of particles [20–23]. However, the particles investigated so far have been electron and nucleon gases. Clearly, the effect of nucleon correlations has not yet been studied. References [20,23] have shown that density and temperature enhance the form factor with standard charge radius, but they do not have a significant effect on the electric and magnetic dipole form factors. Moreover, they can only give a significant contribution if $T/m$ and $\mu/m$ are large, where $T$, $\mu$, and $m$ are the temperature, chemical potential, and mass of the corresponding particles in the thermal bath, respectively [23]. Therefore, the expectation that the temperature and hadron correlations can strongly reduce the electromagnetic properties of neutrinos seems to be unlikely. For simplicity, the random phase approximation (RPA) correlations are still neglected. The importance of neutrino trapping in the supernova dynamical evolution has been pointed out, for example, in Ref. [24]. We choose this kind of matter, because we suspect that the effects of neutrino electromagnetic properties are more pronounced in proton- and electron-rich matter. Different from Ref. [24], which used the standard relativistic mean field (RMF) model to calculate the EOS, in this work we use the RMF model inspired by the effective field theory (E-RMF model) [25].

This paper is organized as follows. Section II consists of a brief review of the matter models used in this work. The analytical results of the neutrino electromagnetic form factor effects on the cross section are given in Sec. III. In Sec. IV, numerical results and their discussions are presented. Finally, the conclusion is given in Sec. V.

## II. MATTER MODELS

To describe nucleon interactions, we use the effective Lagrangian density given in Refs. [25,26]. The wide range of applications of this model have been discussed in detail in Refs. [27,28]. In our work, leptons are assumed to be free (Fermi gas). The framework of our calculation is the relativistic mean field approximation, which means that we treat the nucleon interactions self-consistently. The explicit form of the Lagrangian densities can be seen in Appendix A. By solving the Euler-Lagrange equations for the Lagrangian densities given in Appendix A, the equations of state for

 

TABLE I. Numerical values of coupling constants used in the parameter sets [25,33].

| Parameter | G2 | NL-3 | G2* |
|---|---|---|---|
| $m_S/M$ | 0.554 | 0.541 | 0.554 |
| $g_S/(4\pi)$ | 0.835 | 0.813 | 0.835 |
| $g_V/(4\pi)$ | 1.016 | 1.024 | 1.016 |
| $g_R/(4\pi)$ | 0.755 | 0.712 | 0.938 |
| $\kappa_3$ | 3.247 | 1.465 | 3.247 |
| $\kappa_4$ | 0.632 | −5.668 | 0.632 |
| $\zeta_0$ | 2.642 | 0 | 2.642 |
| $\eta_1$ | 0.650 | 0 | 0.650 |
| $\eta_2$ | 0.110 | 0 | 0.110 |
| $\eta_\rho$ | 0.390 | 0 | 4.490 |

nucleons, mesons, and leptons can be obtained and then used to calculate all matter properties required in this work. The following constraints are used to calculate the fraction of every constituent in matter:

(a) Balance equation for chemical potentials

$$\mu_n + \mu_{\nu_e} = \mu_p + \mu_e, \tag{1}$$

(b) Conservation of charge neutrality

$$\rho_e + \rho_\mu = \rho_p, \tag{2}$$

where the total density of baryon is given by

$$\rho_B = \rho_n + \rho_p, \tag{3}$$

while the fixed electronic-leptonic fraction is defined as

$$Y_{l_e} = \frac{\rho_e + \rho_{\nu_e}}{\rho_B} \equiv Y_e + Y_{\nu_e}. \tag{4}$$

Coupling constants for all parameter sets used in this work are shown in Table I.

## III. EFFECTS OF THE NEUTRINO ELECTROMAGNETIC FORM FACTORS

In this section, we calculate the neutrino-matter cross section, in which the electromagnetic form factors of the neutrino-electron and the weak magnetism of nucleons are explicitly taken into account. We start with the Lagrangian density of neutrino matter interactions for each constituent in the form of

$$\mathcal{L}^j_{\rm int} = \frac{G_F}{\sqrt{2}}\left(\bar\nu\Gamma^\mu_W\nu\right)\left(\bar\psi J^{Wj}_\mu\psi\right) + \frac{4\pi\alpha}{q^2}\left(\bar\nu\Gamma^\mu_{\rm EM}\nu\right)\left(\bar\psi J^{{\rm EM}j}_\mu\psi\right), \tag{5}$$

where $G_F$ and $\alpha$ are the coupling constant of weak interaction and the electromagnetic fine structure constant, respectively, and $j = n, p, e^-, \mu^-$. The parity-violating vertex of neutrino is given by

$$\Gamma^\mu_W = \gamma^\mu(1-\gamma^5), \tag{6}$$

while the electromagnetic properties of Dirac neutrinos are described in terms of four form factors $f_{1\nu}$, $g_{1\nu}$, $f_{2\nu}$, and $g_{2\nu}$, which stand for the Dirac, anapole, magnetic, and electric form factors, respectively. The electromagnetic vertex $\Gamma^\mu_{\rm EM}$ contains electromagnetic form factors [29,30]. Explicitly, it reads

$$\Gamma^\mu_{\rm EM} = f_{m\nu}\gamma^\mu + g_{1\nu}\gamma^\mu\gamma^5 - (f_{2\nu} + ig_{2\nu}\gamma^5)\frac{P^\mu}{2m_e}, \tag{7}$$

where $f_{m\nu} = f_{1\nu} + (m_\nu/m_e)f_{2\nu}$, $P^\mu = k^\mu + k^{\mu\prime}$, and $m_\nu$ and $m_e$ are the neutrino and electron masses, respectively. In the static limit, the reduced Dirac form factor $f_{1\nu}$ and the neutrino anapole form factor $g_{1\nu}$ are related to the vector and axial vector charge radii $\langle R^2_V\rangle$ and $\langle R^2_A\rangle$ through [29]

$$f_{1\nu}(q^2) = \tfrac{1}{6}\langle R^2_V\rangle q^2 \quad \text{and} \quad g_{1\nu}(q^2) = \tfrac{1}{6}\langle R^2_A\rangle q^2, \tag{8}$$

where the neutrino charge radius is defined by $R^2 = \langle R^2_V\rangle + \langle R^2_A\rangle$. In the limit of $q^2 \to 0$, $f_{2\nu}$ and $g_{2\nu}$, respectively, define the neutrino magnetic moment and the Charge Parity (CP) violating electric dipole moment [29,31], i.e.,

$$\mu^m_\nu = f_{2\nu}(0)\mu_B \quad \text{and} \quad \mu^e_\nu = g_{2\nu}(0)\mu_B, \tag{9}$$

where $\mu^2_\nu = (\mu^m_\nu)^2 + (\mu^e_\nu)^2$. The explicit form of $J^{Wj}_\mu$ [4] is given by

$$J^{Wj}_\mu = F^{Wj}_1\gamma_\mu - G^j_A\gamma_\mu\gamma^5 + iF^{Wj}_2\frac{\sigma_{\mu\nu}q^\nu}{2M}, \tag{10}$$

and for $J^{{\rm EM}j}_\mu$ [32] it reads

$$J^{{\rm EM}j}_\mu = F^{{\rm EM}j}_1\gamma_\mu + iF^{{\rm EM}j}_2\frac{\sigma_{\mu\nu}q^\nu}{2M}. \tag{11}$$

In the limit of the photon point, $q^2 \to 0$, the weak form factors $F^W_1$, $G^W_A$, and $F^W_2$ are given in Table II, whereas the electromagnetic form factors of each target $F^{\rm EM}_1$ and $F^{\rm EM}_2$ are given in Table III.

Using the Lagrangian density given by Eq. (5), we can now calculate the differential cross section. Using the standard

TABLE II. Weak form factors in the limit of $q^2 \to 0$ [4]. Here we use $\sin^2\theta_w = 0.231$, $g_A = 1.260$, $\mu_p = 1.793$, and $\mu_n = -1.913$.

| Target | $F^W_1$ | $G_A$ | $F^W_2$ |
|---|---|---|---|
| $n$ | $-0.5$ | $-g_A/2$ | $-1/2(\mu_p - \mu_n) - 2\sin^2\theta_w\mu_n$ |
| $p$ | $0.5 - 2\sin^2\theta_w$ | $g_A/2$ | $1/2(\mu_p - \mu_n) - 2\sin^2\theta_w\mu_p$ |
| $e$ | $0.5 + 2\sin^2\theta_w$ | $1/2$ | 0 |
| $\mu$ | $-0.5 + 2\sin^2\theta_w$ | $-1/2$ | 0 |

TABLE III. Electromagnetic form factors in the limit of $q^2 \to 0$ [32].

| Target | $F^{\rm EM}_1$ | $F^{\rm EM}_2$ |
|---|---|---|
| $n$ | 0 | $\mu_n$ |
| $p$ | 1 | $\mu_p$ |
| $e$ | 1 | 0 |
| $\mu$ | 1 | 0 |

method, we obtain

$$\left(\frac{1}{V}\frac{d^3\sigma}{d^2\Omega' dE'_\nu}\right) = -\frac{1}{16\pi^2}\frac{E'_\nu}{E_\nu}\left[\left(\frac{G_F}{\sqrt{2}}\right)^2 \left(L^{\mu\nu}_\nu \Pi^{\rm Im}_{\mu\nu}\right)^{(W)} + \left(\frac{4\pi\alpha}{q^2}\right)^2 \left(L^{\mu\nu}_\nu \Pi^{\rm Im}_{\mu\nu}\right)^{(\rm EM)} + \frac{8G_F\pi\alpha}{q^2\sqrt{2}}\left(L^{\mu\nu}_\nu \Pi^{\rm Im}_{\mu\nu}\right)^{(\rm INT)}\right]. \quad (12)$$

Here $E_\nu$ and $E'_\nu$ are the initial and final neutrino energies, respectively, $G_F = 1.023\times10^{-5}/M^2$ is the weak coupling, and $M$ is the nucleon mass. The neutrino tensors for the weak contribution is given by

$$L^{\mu\nu(W)}_\nu = 8[2k^\mu k^\nu - (k^\mu q^\nu + k^\nu q^\mu) + g^{\mu\nu}(k\cdot q) - i\epsilon^{\alpha\mu\beta\nu}k_\alpha k'_\beta], \quad (13)$$

while for the electromagnetic contribution,

$$L^{\mu\nu(\rm EM)}_\nu = 4\left(f^2_{m\nu} + g^2_{1\nu}\right)[2k^\mu k^\nu - (k^\mu q^\nu + k^\nu q^\mu) + g^{\mu\nu}(k\cdot q)] - 8if_{m\nu}g_{1\nu}\epsilon^{\alpha\mu\beta\nu}(k_\alpha k'_\beta) - \frac{f^2_{2\nu}+g^2_{2\nu}}{m_e^2}(k\cdot q)[4k^\mu k^\nu - 2(k^\mu q^\nu + q^\mu k^\nu) + q^\mu q^\nu], \quad (14)$$

and for the interference contribution,

$$L^{\mu\nu(\rm INT)}_\nu = 4(f_{m\nu} + g_{1\nu})[2k^\mu k^\nu - (k^\mu q^\nu + k^\nu q^\mu) + g^{\mu\nu}(k\cdot q) - i\epsilon^{\alpha\mu\beta\nu}k_\alpha k'_\beta], \quad (15)$$

with $k$ the initial neutrino four-momentum and $q = (q_0, \vec{q})$ the four-momentum transfer. The polarization tensors $\Pi^{\mu\nu}$ for the weak ($W$), electromagnetic (EM), and interference (INT) terms, which define the target particles, can be written as

$$\Pi^j_{\mu\nu}(q) = -i\int \frac{d^4p}{(2\pi)^4}{\rm Tr}\left[G^j(p)J^j_\mu G^j(p+q)J^j_\nu\right], \quad (16)$$

where $p = (p_0, \vec{p})$ is the corresponding initial four-momentum and $G(p)$ is the target particle propagator. The explicit form for nucleons is given by

$$G^{n,p}(p) = (\not{p}^* + M^*)\left[\frac{1}{p^{*2} - M^{*2} + i\epsilon} + \frac{i\pi}{E^*}\,\delta(p_0^* - E^*)\,\theta\left(p_F^{p,n} - |\vec{p}|\right)\right], \quad (17)$$

where $E^* = E + \Sigma_0$ indicates the nucleon effective energy, and $M^* = E + \Sigma_S$ is the nucleon effective mass. $\Sigma_0$ and $\Sigma_S$ are the scalar and timelike self-energies, respectively. The lepton propagators have similar expressions, only the starred quantities in Eq. (17) are replaced by the free ones. Explicitly, Eq. (16) for each constituent can be written as

$$\Pi^{{\rm Im}(W)j}_{\mu\nu} = \left(F_1^{Wj2} + G_A^{j2}\right)\Pi^{Vj}_{\mu\nu} + \left(G_A^{j2} + \frac{q^2}{2mM}F_1^{Wj}F_2^{Wj}\right)\Pi^{Aj}g_{\mu\nu} - 2\left(F_1^{Wj}G_A^j + \frac{m}{M}F_2^{Wj}G_A^j\right)\Pi^{V-Aj}_{\mu\nu} + \frac{F_2^{Wj2}}{M^2} \times \left[\left(m^2 + \frac{q^2}{4}\right)(q^2 g_{\mu\nu} - q_\mu q_\nu) - \frac{q^2}{8}\Pi^{Vj}_{\mu\nu}\right], \quad (18)$$

$$\Pi^{{\rm Im(EM)}j}_{\mu\nu} = F_1^{{\rm EM}j2}\Pi^{Vj}_{\mu\nu} + \frac{q^2}{2mM}F_1^{{\rm EM}j}F_2^{{\rm EM}j}\Pi^{Aj}g_{\mu\nu} + \frac{F_2^{{\rm EM}j2}}{M^2}\left[\left(m^2 + \frac{q^2}{4}\right) \times (q^2 g_{\mu\nu} - q_\mu q_\nu) - \frac{q^2}{8}\Pi^{Vj}_{\mu\nu}\right], \quad (19)$$

$$\Pi^{{\rm Im(INT)}j}_{\mu\nu} = \left(F_1^{Wj}F_1^{{\rm EM}j} + \frac{q^2}{4M^2}F_2^{Wj}F_2^{{\rm EM}j}\right)\Pi^{Vj}_{\mu\nu} + \left[\frac{F_2^{Wj}F_2^{{\rm EM}j}}{4M^2}\left(1 + \frac{q^2}{4m^2}\right) - \frac{\left(F_1^{Wj}F_2^{{\rm EM}j} + F_2^{Wj}F_1^{{\rm EM}j}\right)}{4mM}\right] \times (q^2 g_{\mu\nu} - q_\mu q_\nu)\Pi^{Aj} + \left(\frac{m}{M}F_2^{{\rm EM}j}G_A^j - F_1^{{\rm EM}j}G_A^j\right)\Pi^{V-Aj}_{\mu\nu}, \quad (20)$$

where for $j = n$, $p$ (nucleons), $m$ is equal to $M^*$ and $M$ is the nucleon mass; while for $j = e^-$, $\mu^-$ (leptons), $m$ is equal to $M$, the lepton mass.

Due to the current conservation and translational invariance, the vector polarization $\Pi^{{\rm Im}V}_{\mu\nu}$ of every contribution consists of two independent components which we choose to be in the frame of $q^\mu \equiv (q_0, |\vec{q}|, 0, 0)$, i.e.,

$$\Pi_T = \Pi^V_{22} = \Pi^V_{33},$$
$$\Pi_L = -\left(q^2_\mu/|\vec{q}|^2\right)\Pi^V_{00}.$$

The axial vector and the mixed pieces are found to be

$$\Pi^{{\rm Im}(V-A)}_{\mu\nu}(q) = i\epsilon_{\alpha\mu 0\nu}q_\alpha \Pi_{VA}. \quad (21)$$

The explicit forms of $\Pi_T$, $\Pi_L$, $\Pi_{VA}$, and $\Pi_A$ for nucleons are [33]

$$\Pi_T = \frac{1}{4\pi|\vec{q}|}\left[\left(M^{*2} + \frac{q^2}{4|\vec{q}|^2} + \frac{q^2}{2}\right)(E_F - E^*) + \frac{q_0 q^2}{2|\vec{q}|}\left(E_F^2 - E^{*2}\right) + \frac{q^2}{3|\vec{q}|}\left(E_F^3 - E^{*3}\right)\right], \quad (22)$$

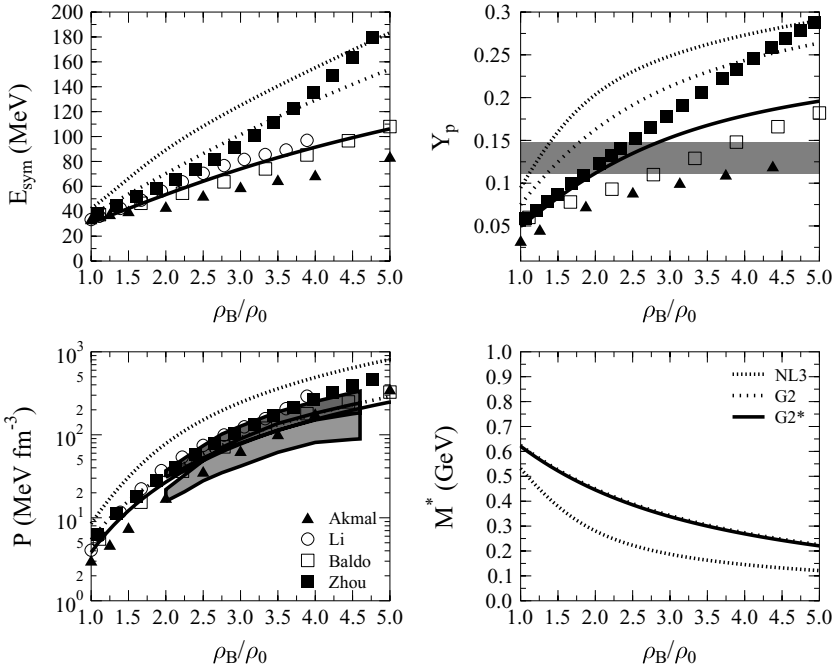


FIG. 1. Performance of the models. G2 is the standard parameter set of the E-RMF model, G2* is the parameter set of the E-RMF model with an adjusted isovector-vector channel (see Appendix A for details). NL3 is the parameter set of the standard RMF model. The symmetry energy $E_{\rm sym}$ of nuclear matter is shown in the upper left panel. The pressure $P$ and $M^*$ of PNM are given in the lower left and the lower right panels, respectively, and the neutron star proton fraction predictions can be seen in the upper right panel. Shaded region in the $P$ panel corresponds to experimental data of Danielewicz *et al.* [34]; whereas in the $Y_p$ panel it corresponds to the proton fraction threshold for direct URCA process.

$$\Pi_L = \frac{q^2}{2\pi|\vec{q}|^3}\left[\frac{1}{4}(E_F - E^*) + \frac{q_0}{2}\left(E_F^2 - E^{*2}\right) + \frac{1}{3}\left(E_F^3 - E^{*3}\right)\right], \tag{23}$$

$$\Pi_{VA} = \frac{iq^2}{8\pi|\vec{q}|^3}\left[\left(E_F^2 - E^{*2}\right) + q_0(E_F - E^*)\right]. \tag{24}$$

$$\Pi_A = \frac{i}{2\pi|\vec{q}|}M^{*2}(E_F - E^*). \tag{25}$$

For leptons, they also have similar expressions, only the starred quantities in Eqs. (22)–(25) are replaced by the free ones. Thus, the analytical form of Eq. (12) can be obtained from the contraction of every polarization and neutrino tensor couple ($L^{\mu\nu}\Pi_{\mu\nu}$) mentioned previously. The results are

$$\left(L_\nu^{\mu\nu}\Pi_{\mu\nu}^{\rm Im}\right)^{(W)} = -8q^2 \sum_{j=n,p,e^-,\mu^-}\left[A_W^j\left(\Pi_L^j + \Pi_T^j\right) + B_{1\rm W}^j\Pi_T^j + B_{2\rm W}^j\Pi_A^j + C_W^j\Pi_{VA}^j\right], \tag{26}$$

$$\left(L_\nu^{\mu\nu}\Pi_{\mu\nu}^{\rm Im}\right)^{(\rm EM)} = q^2 \sum_{j=n,p,e^-,\mu^-}\left[A_{\rm EM}^j\left(\Pi_L^j + \Pi_T^j\right) + B_{1\rm EM}^j\Pi_T^j + B_{2\rm EM}^j\Pi_A^j\right], \tag{27}$$

$$\left(L_\nu^{\mu\nu}\Pi_{\mu\nu}^{\rm Im}\right)^{(\rm INT)} = -4q^2 \sum_{j=n,p,e^-,\mu^-}\left[A_{\rm INT}^j\left(\Pi_L^j + \Pi_T^j\right) + B_{1\rm INT}^j\Pi_T^j + B_{2\rm INT}^j\Pi_A^j + C_{\rm INT}^j\Pi_{VA}^j\right], \tag{28}$$

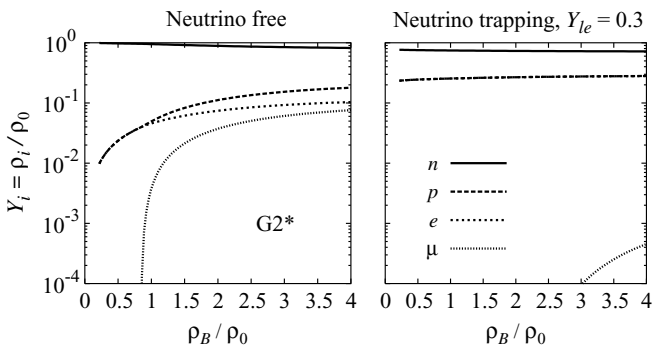


FIG. 2. Relative fraction of the individual constituent of the nonstrange matter as a function of the ratio between baryon and saturation densities. Calculations used the G2* parameter set.

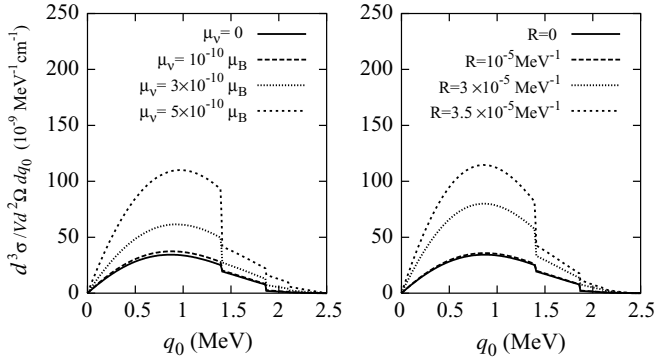


FIG. 3. Total differential cross section as a function of $q_0$, calculated at fixed $q_1 = 2.5$ MeV, $E_\nu = 5$ MeV in neutrinoless matter. In the left panel, $R$ is fixed to zero and $\mu_\nu$ is varied; in the right panel, $\mu_\nu$ is fixed to zero and $R$ is varied.

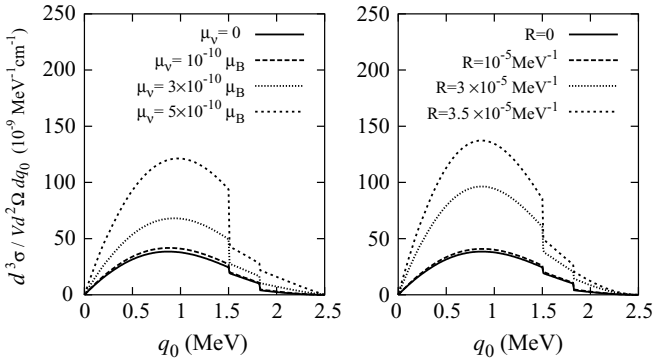


FIG. 4. Same as in Fig. 3, but for the case where neutrinos are trapped in matter with $Y_{l_e} = 0.3$.

where the functions in front of every polarization term of Eqs. (26)–(28) are given by

$$
\begin{aligned}
A^j_W &= \left(\frac{2E(E-q_0)+\frac{1}{2}q^2}{|\vec{q}|^2}\right)\left[F_1^{Wj2}+G_A^{j2}-\frac{F_2^{Wj2}q^2}{4M^2}\right],\\
B^j_{1W} &= \left[F_1^{Wj2}+G_A^{j2}-\frac{F_2^{Wj2}q^2}{4M^2}\right],\\
B^j_{2W} &= -\left[G_A^{j2}+\frac{q^2}{2mM}F_1^{Wj}F_2^{Wj}-\frac{F_2^{Wj2}q^2}{4M^2}\left(1+\frac{q^2}{4m^2}\right)\right],\\
C^j_W &= -2(2E-q_0)\left[F_1^{Wj}G_A^j+\frac{m}{M}F_2^{Wj}G_A^j\right],
\end{aligned}
\tag{29}
$$

for the weak contributions, and

$$
\begin{aligned}
A^j_{\rm EM} &= \left[\left(\frac{2E(E-q_0)+\frac{1}{2}q^2}{|\vec{q}|^2}\right)(bq^2-a)+\frac{1}{2}bq^2\right]\\
&\quad\times\left[F_1^{{\rm EM}j2}-\frac{F_2^{{\rm EM}j2}q^2}{4M^2}\right],\\
B^j_{1\rm EM} &= -\frac{1}{2}(bq^2+a)\left[F_1^{{\rm EM}j2}-\frac{F_2^{{\rm EM}j2}q^2}{4M^2}\right],\\
B^j_{2\rm EM} &= \frac{1}{2}(bq^2+a)\left[\frac{q^2}{2mM}F_1^{{\rm EM}j}F_2^{{\rm EM}j}\right.\\
&\quad\left.-\frac{F_2^{{\rm EM}j2}q^2}{4M^2}\left(1+\frac{q^2}{4m^2}\right)\right],
\end{aligned}
\tag{30}
$$

for the electromagnetic contributions, and

$$
\begin{aligned}
A^j_{\rm INT} &= c\left(\frac{2E(E-q_0)+\frac{1}{2}q^2}{|\vec{q}|^2}\right)\\
&\quad\times\left[F_1^{Wj}F_1^{{\rm EM}j}+\frac{q^2}{4M^2}F_2^{Wj}F_2^{{\rm EM}j}\right],\\
B^j_{1\rm INT} &= c\left[F_1^{Wj}F_1^{{\rm EM}j}+\frac{q^2}{4M^2}F_2^{Wj}F_2^{{\rm EM}j}\right],\\
B^j_{2\rm INT} &= -cq^2\left[\frac{F_2^{Wj}F_2^{{\rm EM}j}}{4M^2}\left(1+\frac{q^2}{4m^2}\right)\right.\\
&\quad\left.-\frac{\left(F_1^{Wj}F_2^{{\rm EM}j}+F_2^{Wj}F_1^{{\rm EM}j}\right)}{4mM}\right],\\
C^j_{\rm INT} &= c(2E-q_0)\left[\frac{m}{M}F_2^{{\rm EM}j}G_A^j-F_1^{{\rm EM}j}G_A^j\right],
\end{aligned}
\tag{31}
$$

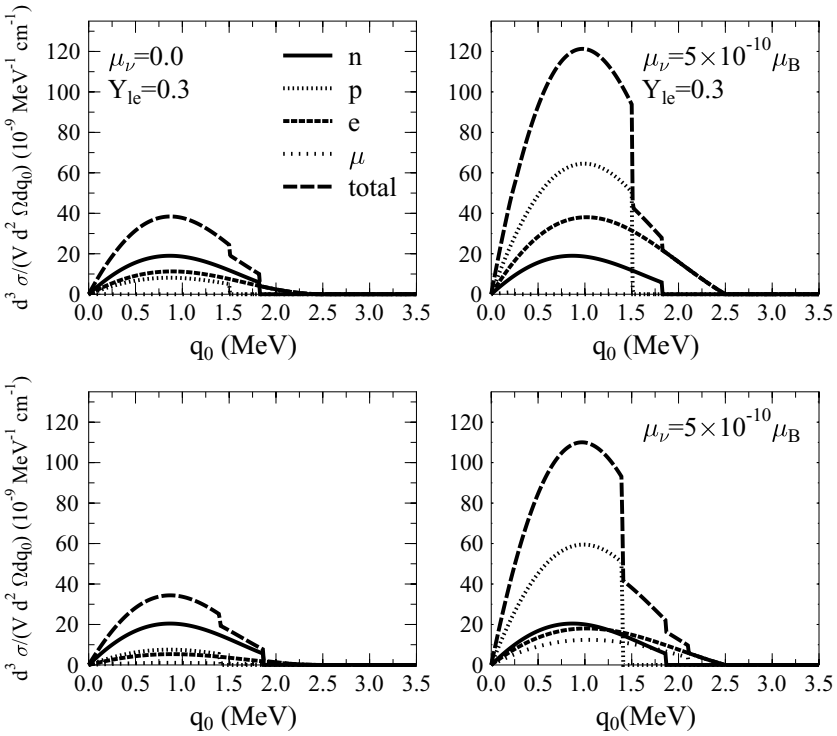


FIG. 5. Total differential cross section and contributions from individual constituents as a function of $q_0$ obtained at fixed $q_1 = 2.5$ MeV, $E_\nu = 5$ MeV, and $\rho_B = 2.5\rho_0$; charge radius $R = 0$.

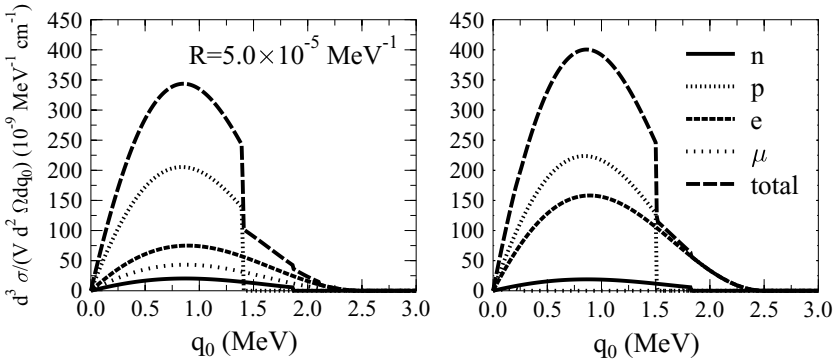


FIG. 6. Same as Fig. 5, but for $\mu_\nu$ set to zero and $R = 5 \times 10^{-5}\,\mathrm{MeV}^{-1}$. Neutrinos are absent in the left panel; $Y_{l_e} = 0.3$ in the right panel.

for the interference contributions. The constants $a$, $b$, and $c$ are defined as

$$a = 4\left(f_{m\nu}^2 + g_{1\nu}^2\right), \quad b = \frac{f_{2\nu}^2 + g_{2\nu}^2}{m_e^2}, \quad c = f_{m\nu} + g_{1\nu},$$

where these neutrino form factors $f_{m\nu}$, $g_{1\nu}$, $f_{2\nu}$, and $g_{2\nu}$ are related to the neutrino-electron dipole moment and charge radius through Eqs. (8) and (9).

## IV. NUMERICAL RESULTS AND DISCUSSIONS

Before investigating the sensitivity of the neutrino-matter differential cross section to the neutrino electromagnetic form factors, we show the predictions of the nuclear model used in the calculation (G2* parameter set) at high density in Figs. 1 and 2. Figure 1 reveals that the G2* parameter set has the softest $E_{\mathrm{sym}}$ compared to the other parameter sets (G2 and NL3). As a consequence, it has the highest threshold density for the direct

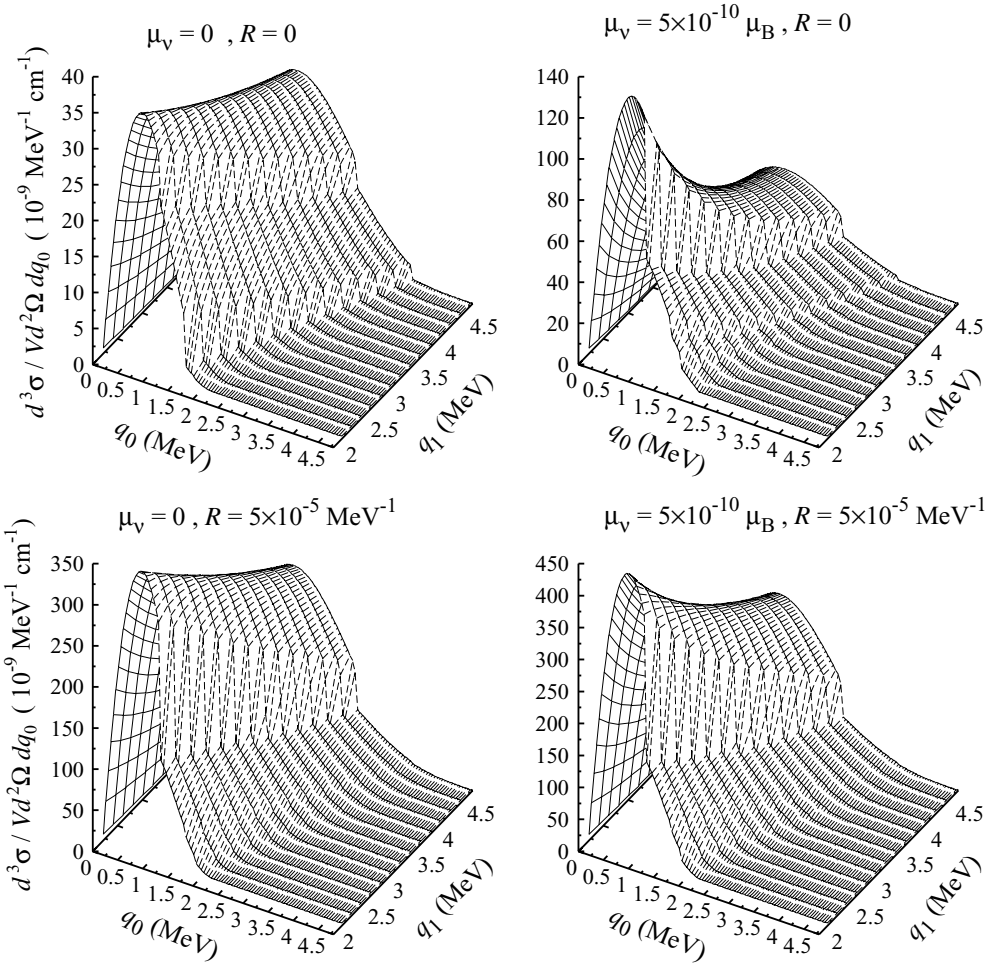


FIG. 7. Total differential cross sections as functions of $q_0$ and $q_1$ for the case where neutrinos are absent, $\rho_B$ is fixed to $2.5\rho_0$, and $E_\nu = 5$ MeV.

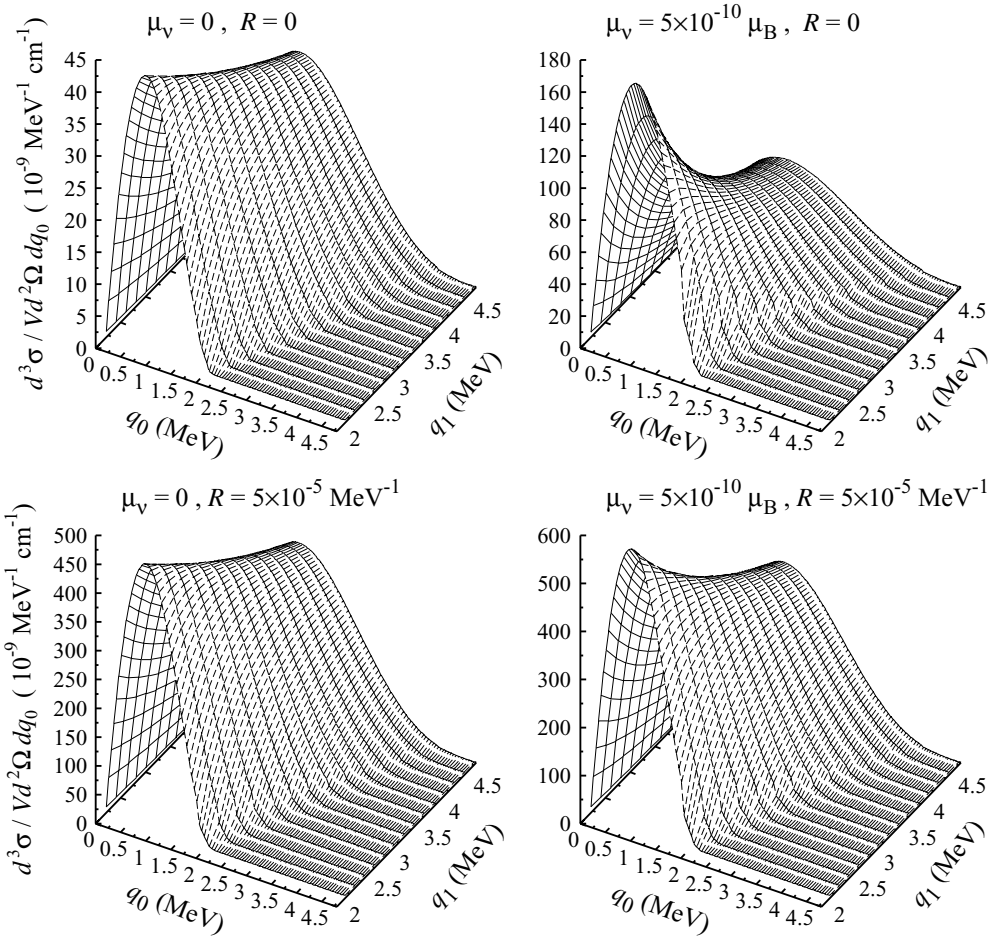


FIG. 8. Same as Fig. 7, but for fixed $\rho_B = 5\rho_0$.

URCA process compared to the other parameter sets. On the other hand, G2* and G2 have a similar trend in the pure neutron matter (PNM) EOS and effective mass $M^*$, i.e., soft EOS and high value of $M^*$ at high densities. This fact indicates that the neutron star properties (masses, radii, etc.) predicted by G2* and G2 are quite similar. For comparison, we also show the results from variational calculation of Akmal *et al.* [35], the Dirac-Brueckner-Hartree-Fock (DBHF) calculation of Li *et al.* [36], the Brueckner-Hartree-Fock (BHF) with AV14 potential plus the phenomenological 3BF of Baldo *et al.* [37] and the recent BHF calculation with the meson-exchange microscopic model of Zhou *et al.* [38]. We learn that G2* has an agreement in proton fraction $Y_p$ with the recent BHF calculation of Zhou *et al.* [38] at $\rho \leqslant 2.5\rho_B$; but at large densities, their calculation predicts a larger $Y_p$. On the other hand, and in general, Baldo *et al.* [37] and Akmal *et al.* [35] obtained a relatively much smaller $Y_p$ than that of G2*. The $Y_p$ differences in all models originate from the differences in the predicted $E_{\rm sym}$.

The left panel of Fig. 2 shows the relative fraction of every constituent in the case that neutrinos are absent, while the right panel shows the case when neutrinos are trapped. We obtain a similar conclusion as in Ref. [24], i.e., when Fermi momentum of the electrons reaches the muon mass, muons begin to appear, and then the proton and electron fraction curves are split into two different paths. The threshold for muon production occurs just below the saturation density. In the case that neutrinos are trapped, for example, with $Y_{l_e} = 0.3$, the threshold is shifted toward higher densities. This displacement is even larger for the E-RMF model ($\rho = 3\rho_0$) than the result of Ref. [24] ($\rho = 2\rho_0$). This similar finding leads to a conclusion similar to that drawn in Ref. [24]; i.e., the EOS of matter with neutrino trapping is softer than the case where neutrinos are absent. This fact leads to a very important consequence for the physics of supernovae explosions [24].

Figures 3 and 4 reveal [14] that a significant difference between total (including neutrino-electron electromagnetic properties) and weak differential cross sections in electron gas, starting more or less from $\mu_\nu > 10^{-10}\mu_B$ and $R > 10^{-5}\,\mathrm{MeV}^{-1}$, also occurs in dense matter. If neutrinos are present in matter, then the threshold values of $\mu_\nu$ and $R$ become more or less similar to the case where neutrinos are absent. The increment in the cross section right after the threshold is relatively faster for the neutrino trapping case than for the case where neutrinos are absent. The rapid increment of the transversal and longitudinal cross sections right after threshold seems to be the reason for this fact.

In Figs. 5 and 6, we show the total differential cross sections along with individual contributions of their constituents as

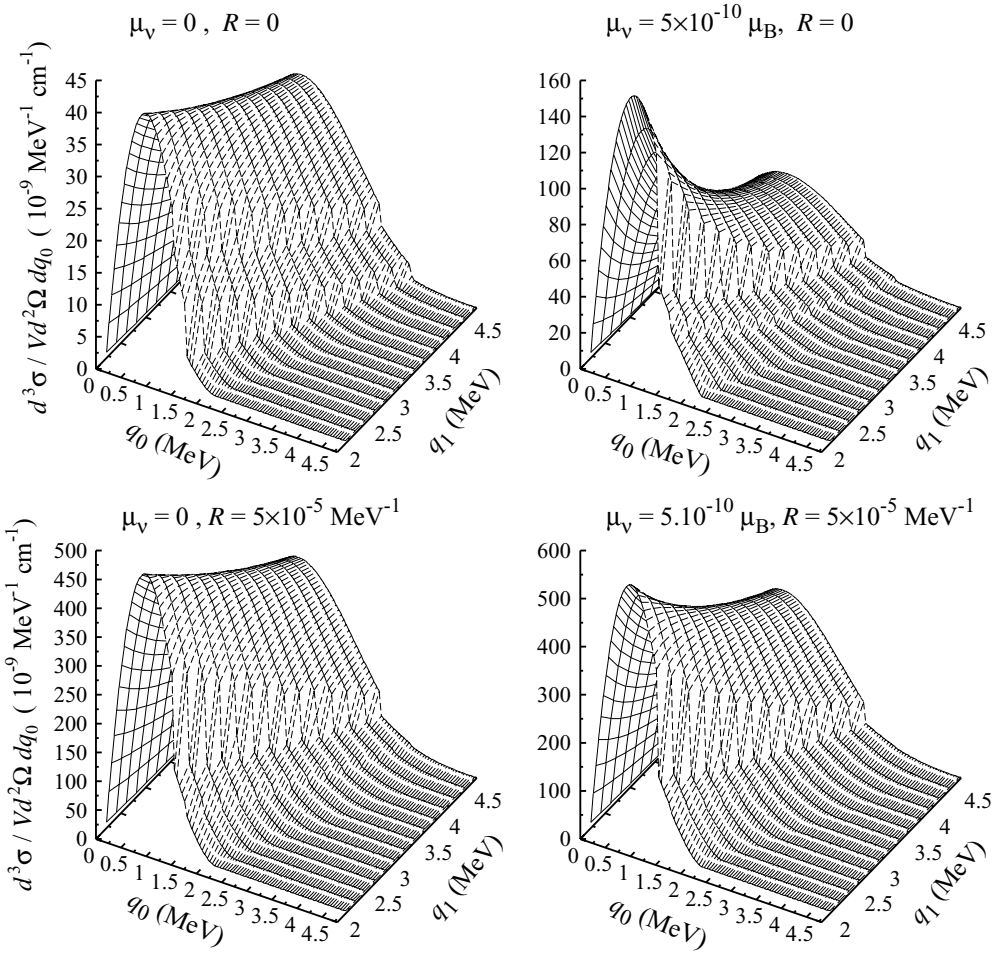


FIG. 9. Same as Fig. 7, but for $Y_{l_e} = 0.3$.

a function of the energy transfer $q_0$ at a fixed momentum transfer $q_1 = 2.5$ MeV, neutrino energy $E_\nu = 5$ MeV, and baryon density $\rho_B = 2.5\rho_0$. In Fig. 5, we set $R$ and $\mu_\nu$ to zero in the left panels, while $\mu_\nu = 5 \times 10^{-10}\,\mu_B$ in the right panels. The results in lower panels are obtained if neutrinos are absent, while those in upper panels are obtained when neutrinos are trapped. In Fig. 6, we set $\mu_\nu = 0$ and $R = 5 \times 10^{-5}\,\mathrm{MeV}^{-1}$. The left panel exhibits the case where neutrinos are absent, and the right panel shows the case where neutrinos are trapped.

From the lower left panel of Fig. 5 (the standard weak interaction cases, where neutrinos are absent), we can see that the proton contribution is larger than the electron one; but, on the contrary, from the upper left panel of Fig. 5 (where neutrinos are trapped), the proton contribution is smaller than the electron one. Both contributions increase if the neutrinos are present, as shown in the upper left panel. It can also be seen that muons play almost no role in this case. However, since neutron contributions are dominant in both cases and they have more or less the same cross section magnitude, the difference between neutrino absent and neutrino trapped in matter in each individual contribution does not significantly show up in the total differential cross section.

In order to see the effect more clearly, we take $\mu_\nu = 5 \times 10^{-10}\,\mu_B$ in the case of nonzero neutrino dipole moment. Obviously, this value is larger than its laboratory bound ($\mu_\nu = 1.0 \times 10^{-10}\,\mu_B$) as well as the bound from astrophysical consideration ($3.0 \times 10^{-12}\,\mu_B$). The result can be seen in the lower right panel of Fig. 5 (for the neutrino absent case), where we can see that the proton contribution is larger than the neutron one and the electron contribution has a similar order to the neutron one, while the muons start to make a significant contribution. On the other hand, in the neutrino trapping case (upper left panel, Fig. 5), muons make almost no contribution. Contributions from protons and electrons are larger than those from neutrons in this case. The different number of particle distributions of each constituent between both cases leads to a difference in the total differential cross sections. It can be seen in Fig. 6 that a similar situation happens for the case of $R = 5.0 \times 10^{-5}\,\mathrm{MeV}^{-1}$ with $\mu_\nu = 0$. This means that in contrast to the calculation based on the standard weak interaction, the cross section calculated by including neutrino electromagnetic properties is very sensitive to the particle number of each constituent.

To see how sensitive the calculated total cross section is to the neutrino electromagnetic properties, we plot the total differential cross sections as functions of the energy transfer $q_0$ and momentum transfer $q_1$ for baryon density $\rho_B = 2.5\rho_0$ in Figs. 7 and 9, and for $\rho_B = 5\rho_0$ in Figs. 8 and 10. Figures 7

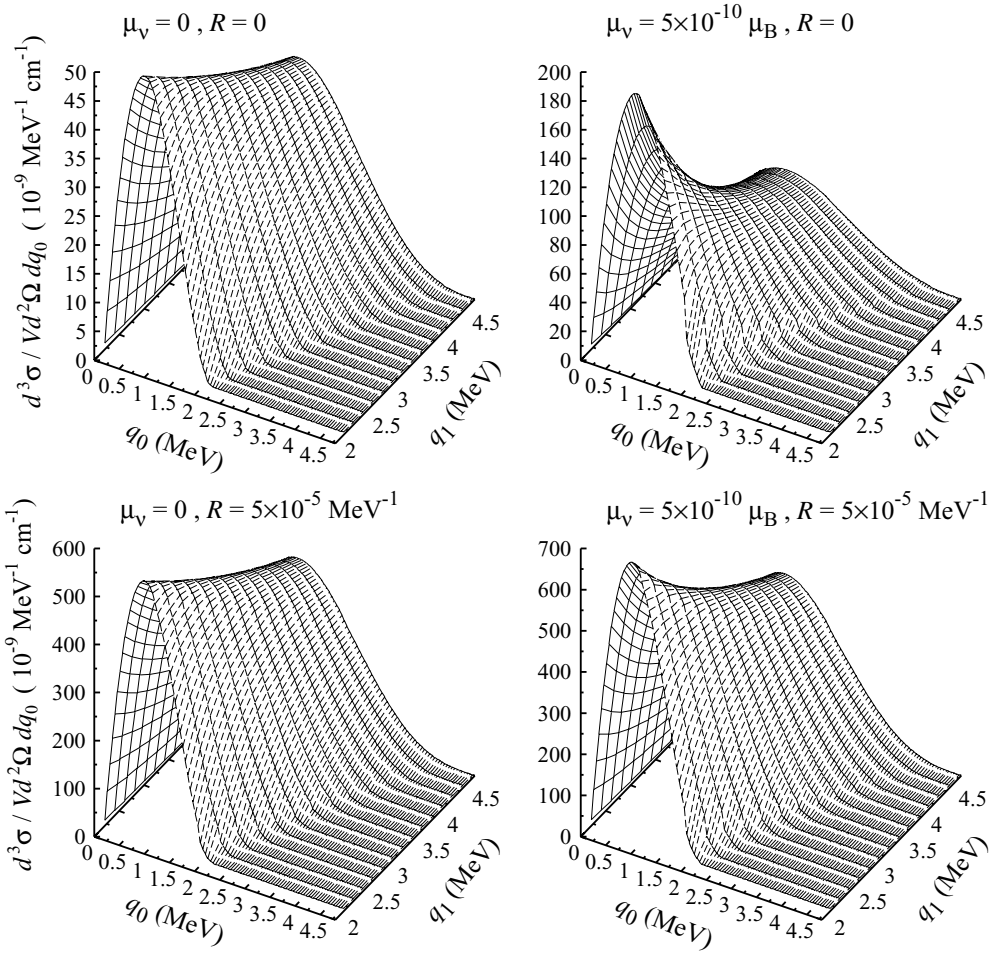


FIG. 10. Same as Fig. 9, but for $\rho_B = 5\rho_0$.

and 8 show the results in the neutrino absent case; Figs. 9 and 10 show the results when neutrinos are present.

Clearly from Fig. 7, for fixed $\mu_\nu$, in general, the trends of cross sections between $R = 0$ and $R = 5.0 \times 10^{-5}\,\mathrm{MeV}^{-1}$ are quite similar. Only in the region of $q_0 \simeq 1$–2 MeV and $q_1 \simeq 2$–4.5 MeV to the shapes of cross sections seem to be quite different. The magnitudes of both cross sections are different because of the quite large value of $R$. However, in the case of fixed $R$ and $\mu_\nu = 5.0 \times 10^{-10}\,\mu_B$, the trend and magnitude of the total cross section change. The cross section decreases when $q_1$ increases. In the upper right panel of Fig. 7, we see that this decrement can be slowed down if the charge radius is set to a nonzero value (e.g., $5.0 \times 10^{-5}\,\mathrm{MeV}^{-1}$). The effect of nonzero neutrino dipole moment appears more dominantly at smaller values of momentum transfer $q_1$ and energy transfer $q_0$, which is due to the role of massless photon propagators in the electromagnetic interaction. On the contrary, the weak contribution becomes more dominant at larger values of $q_1$ and $q_0$.

By comparing Figs. 7 and 8, we can see that in higher densities (i.e., $\rho_B = 5.0\rho_0$) the magnitude of each cross section becomes significantly large and, as a consequence, the differences between the total and the weak cross sections become more pronounced. Furthermore, the shapes of the cross sections become smoother in this case.

The case of trapped neutrino (e.g., $Y_{l_e} = 0.3$) in Figs. 9 and 10 shows significant difference between total and weak cross sections because of the larger cross section, as we expected. Nevertheless, there is no indication that the change in the cross section trend is due to the more pronounced difference of the role of each constituent in the higher density. The difference in the shapes of cross sections calculated by including and excluding electromagnetic form factors also appears in the region of $q_0 \simeq 1$–2 MeV and $q_1 \simeq 2$–4.5 MeV for low densities (i.e., $\rho_B = 2.5\rho_0$), albeit with a different trend.

In addition, if we consider the upper bound of the neutrino-muon dipole moment which is given by $\mu_\nu < 7.4 \times 10^{-10}\,\mu_B$ [39,40], besides the weak magnetism term as investigated by Ref. [4], it seems from the above discussion that the neutrino-muon electromagnetic properties might give additional effects to the neutrino muon and its anti-neutrino mean free path difference in neutron-rich matter. How significant the effects are should be quantitatively checked by a real calculation.

## V. CONCLUSIONS AND OUTLOOK

In conclusion, we have studied the sensitivity of the neutrino cross section to the neutrino electromagnetic properties.

In our calculations, we use the G2* parameter set of the E-RMF model to describe matter. This parameter set predicts a soft EOS at high density and has $\rho_B = 2.5\rho_0$ that coincides with the direct URCA process threshold. The calculation has been performed for cases in which neutrinos are trapped and absent in matter. We found that in the nonstrange stellar matter, the electromagnetic form factor has an important role in the neutrino-electron matter cross section if $\mu_\nu > 10^{-10}\mu_B$ and $R > 10^{-5}\,\mathrm{MeV}^{-1}$. Furthermore, the effects of the neutrino electromagnetic form factors on the cross sections are more pronounced at higher densities.

Matter with trapped neutrinos, such supernovae, are more sensitive to the presence of neutrino electromagnetic properties. This is because matter with trapped neutrinos have larger fractions of protons and electrons than those without neutrinos. Although we have found that the role of neutrino electromagnetic properties in the neutrino-electron matter interaction is not too crucial, this would not be the case if we considered the bound of the neutrino-muon dipole moment given by Refs. [39,40].

With increasing density of the protoneutron star, strangeness can be liberated and face up in the the filling of the hyperon Fermi seas and/or in the creation of kaon condensates. Occurrence of these exotics in protoneutron star interiors will enhance the neutrino scattering rate and may also have interesting observational consequences, such as softening the EOS, changing nucleon isospin composition in the star matter evolution, or enhancing neutrino emission processes in the neutron star matter evolution, as extensively discussed in Refs. [19,41–48]. Furthermore, depending on the temperature and model used, baryon correlations can also reduce the scattering rate [4,6,8,10,13]. Therefore, an extension of this calculation by including the strange matter, RPA correlation, and a more general condition, i.e., finite temperature, might also be interesting and quite relevant to consider in the future.

## ACKNOWLEDGMENT

We acknowledge P. Danielewicz for his kindness in giving us his experimental data.

## APPENDIX A: LAGRANGIAN DENSITIES

The effective Lagrangian density of the E-RMF model is [25,26]

$$\mathcal{L}^{\mathrm{nuc}} = \mathcal{L}_N + \mathcal{L}_M, \tag{A1}$$

where the nucleon part, up to order $\nu = 3$, has the form

$$\mathcal{L}_N = \bar{\psi}[i\gamma^\mu(\partial_\mu + i\bar{v}_\mu + ig_\rho\bar{b}_\mu + ig_\omega V_\mu) + g_A\gamma^\mu\gamma^5\bar{a}_\mu - M + g_\sigma\sigma]\psi - \frac{f_\rho g_\rho}{4M}\bar{\psi}\bar{b}_{\mu\nu}\sigma^{\mu\nu}\psi, \tag{A2}$$

with

$$\psi = \begin{pmatrix} p \\ n \end{pmatrix}, \quad \bar{v}_\mu = -\frac{i}{2}(\bar{\xi}^\dagger\partial_\mu\bar{\xi} + \bar{\xi}\partial_\mu\bar{\xi}^\dagger) = \bar{v}_\mu^\dagger, \tag{A3}$$

$$\bar{a}_\mu = -\frac{i}{2}(\bar{\xi}^\dagger\partial_\mu\bar{\xi} - \bar{\xi}\partial_\mu\bar{\xi}^\dagger) = \bar{a}_\mu^\dagger, \tag{A4}$$

$$\bar{\xi} = \exp(i\bar{\pi}(x)/f_\pi), \quad \bar{\pi}(x) = \tfrac{1}{2}\vec{\tau}\cdot\vec{\pi}(x), \tag{A5}$$

$$\bar{\pi}(x) = \tfrac{1}{2}\vec{\tau}\cdot\vec{\pi}(x), \tag{A6}$$

$$\bar{b}_{\mu\nu} = D_\mu\bar{b}_\nu - D_\nu\bar{b}_\mu + ig_\rho[\bar{b}_\mu, \bar{b}_\nu], \quad D_\mu = \partial_\mu + i\bar{v}_\mu, \tag{A7}$$

$$V_{\mu\nu} = \partial_\mu V_\nu - \partial_\nu V_\mu, \tag{A8}$$

$$\sigma^{\mu\nu} = \tfrac{1}{2}[\gamma^\mu, \gamma^\nu]. \tag{A9}$$

Here, $p, n$, and $M$ are the proton field, neutron field, and nucleon mass; and $\sigma, \vec{\pi}, V^\mu$, and $\vec{b}^\mu$ are the $\sigma, \pi, \omega$, and $\rho$ meson fields, respectively. The meson contribution, up to order $\nu = 4$, reads

$$\begin{aligned}\mathcal{L}_M = {} & \frac{1}{4}f_\pi^2\mathrm{Tr}(\partial_\mu\bar{U}\partial^\mu\bar{U}^\dagger) + \frac{1}{4}f_\pi^2\mathrm{Tr}(\bar{U}\bar{U}^\dagger - 2) \\ & + \frac{1}{2}\partial_\mu\sigma\partial^\mu\sigma - \frac{1}{2}\mathrm{Tr}(\bar{b}_{\mu\nu}\bar{b}^{\mu\nu}) - \frac{1}{4}V_{\mu\nu}V^{\mu\nu} \\ & - g_{\rho\pi\pi}\frac{2f_\pi^2}{m_\rho^2}\mathrm{Tr}(\bar{b}_{\mu\nu}\bar{v}^{\mu\nu}) + \frac{1}{2}\left(1 + \eta_1\frac{g_\sigma\sigma}{M}\right. \\ & \left. + \frac{\eta_2}{2}\frac{g_\sigma^2\sigma^2}{M^2}\right)m_\omega^2 V_\mu V^\mu + \frac{1}{4!}\zeta_0 g_\omega^2(V_\mu V^\mu)^2 \\ & + \left(1 + \eta_\rho\frac{g_\sigma\sigma}{M}\right)m_\rho^2\mathrm{Tr}(\bar{b}_\mu\bar{b}^\mu) \\ & - m_\sigma^2\sigma^2\left(1 + \frac{\kappa_3}{3!}\frac{g_\sigma\sigma}{M} + \frac{\kappa_4}{4!}\frac{g_\sigma^2\sigma^2}{M^2}\right),\end{aligned} \tag{A10}$$

where

$$\bar{U} = \bar{\xi}^2, \ \ \bar{v}_{\mu\nu} = \partial_\mu\bar{v}_\nu - \partial_\nu\bar{v}_\mu + i[\bar{v}_\mu, \bar{v}_\nu] = -i[\bar{a}_\mu, \bar{a}_\nu]. \tag{A11}$$

In the mean field approximation, $\pi$ meson makes no contribution. If we set $\eta_1, \eta_2, \zeta_0, \eta_\rho$, and $f_\rho$ equal to zero, we will obtain the same nucleon and meson equations as in the standard RMF models [49–51].

To achieve a softer density dependence of the nuclear matter symmetry energy of the standard RMF model, Refs. [33,52] add isovector-vector nonlinear terms in the Lagrangian density. In this paper, a similar procedure as in Refs. [33,52] is adopted. Since in the E-RMF model the isovector-vector nonlinear term is already present, the density dependence of the nuclear matter symmetry energy can be adjusted without adding new isovector nonlinear terms. Thus, we only adjust $g_\rho$ and $\eta_\rho$ but maintain the requirement that the symmetry energy at $k_F = 1.14$ fm should have the same value at $E_{\mathrm{sym}} = 24.1$ MeV. The argument behind this procedure is explained in detail in Refs. [33,52]. For leptons, we use the following free Lagrangian density:

$$\sum_{l=e^-,\,\mu^-,\,\nu}\bar{l}(\gamma^\mu\partial_\mu - m_l)l. \tag{A12}$$

[1] S. Reddy, M. Prakash, and J. M. Lattimer, Phys. Rev. D **58**, 013009 (1998); and references therein.
[2] R. Niembro, P. Bernardos, M. Lopez-Quelle, and S. Marcos, Phys. Rev. C **64**, 055802 (2001).
[3] P. T. P. Hutauruk, C. K. Williams, A. Sulaksono, and T. Mart, Phys. Rev. C **70**, 068801 (2004).
[4] C. J. Horowitz and M. A. Pérez-García, Phys. Rev. C **68**, 025803 (2003).
[5] L. Mornas, Nucl. Phys. **A721**, 1040 (2003).
[6] L. Mornas and A. Perez, Eur. Phys. J. A **13**, 383 (2002).
[7] S. Reddy, M. Prakash, J. M. Lattimer, and J. A. Pons, Phys. Rev. C **59**, 2888 (1999).
[8] C. J. Horowitz and K. Wehberger, Nucl. Phys. **A531**, 665 (1991); Phys. Lett. **B266**, 236 (1991).
[9] S. Yamada and H. Toki, Phys. Rev. C **61**, 015803 (1999).
[10] C. Shen, U. Lombardo, N. Van Giai, and W. Zuo, Phys. Rev. C **68**, 055802 (2003).
[11] J. Margueron, J. Navarro, and N. Van Giai, Nucl. Phys. **A719**, 169 (2003).
[12] D. Chandra, A. Goyal, and K. Goswami, Phys. Rev. D **65**, 053003 (2002).
[13] S. Cowell and V. R. Pandharipande, Phys. Rev. C **70**, 035801 (2004).
[14] C. K. Williams, P. T. P. Hutauruk, A. Sulaksono, and T. Mart, Phys. Rev. D **71**, 017303 (2005).
[15] Z. Daraktchieva *et al*. (MUNU Collaboration), Phys. Lett. **B564**, 190 (2003).
[16] G. G. Raffelt, Phys. Rev. Lett. **64**, 2856 (1990); Phys. Rep. **320**, 319 (1999), and references therein.
[17] R. C. Allen *et al*., Phys. Rev. D **47**, 11 (1993).
[18] A. Friedland, hep-ph/0505165 (2005), and references therein.
[19] Guo Hua, Chen Yanjun, Liu Bo, Zhao Qi, and Liu Yuxin, Phys. Rev. C **68**, 035803 (2003) and references therein.
[20] J. F. Nieves, Phys. Rev. D **70**, 073001 (2004) and references therein.
[21] J. F. Nieves and P. B. Pal, Phys. Rev. D **49**, 1398 (1994).
[22] R. F. Sawyer, Phys. Rev. D **46**, 1180 (1992).
[23] S. S. Masood, Phys. Rev. D **48**, 3250 (1993).
[24] M. Chiapparini, H. Rodrigues, and S. B. Duarte, Phys. Rev. C **54**, 936 (1996).
[25] R. J. Furnstahl, B. D Serot, and H. B. Tang, Nucl. Phys. **A598**, 539 (1996); **A615**, 441 (1997).
[26] P. Wang, Phys. Rev. C **61**, 054904 (2000).
[27] T. Sil, S. K. Patra, B. K. Sharma, M. Centelles, and X. Vinás, in *Focus on Quantum Field Theory*, edited by O. Kovras (Nova Science Publishers, Inc., New York, 2005).
[28] P. Arumugam, B. K. Sharma, P. K. Sahu S. K. Patra, T. Sil, M. Centelles, and X. Vinãs, Phys. Lett. **B601**, 51 (2004).
[29] B. K. Kerimov, M. Ya Safin, and H. Nazih, Izv. Akad. Nauk. SSSR. Fiz **52**, 136 (1998).
[30] A. M. Mourao, J. Pulido, and J. P. Ralston, Phys. Lett. **B285**, 364 (1992).
[31] E. Nardi, AIP Conf. Proc. **670**, 118 (2003); M. Hirsch, E. Nardi, and D. Restrepo, Phys, Rev. D **67**, 033005 (2003).
[32] P. Vogel and J. Engel, Phys. Rev. D **39**, 3378 (1989).
[33] C. J. Horowitz and J. Piekarewicz, Phys. Rev. Lett. **86**, 5647 (2001).
[34] P. Danielewicz, R. Lacey, and W. G. Lynch, Science **298**, 1592 (2002).
[35] A. Akmal, V. R. Pandharipande, and D. G. Ravenhall, Phys. Rev. C **58**, 1804 (1998).
[36] G. Q. Li, R. Machleidt, and R. Brockmann, Phys. Rev. C **45**, 2782 (1992).
[37] M. Baldo, I. Bombaci, and G. F. Burgio, Astron. Astrophys. **328**, 274 (1997).
[38] X. R. Zhou, G. F. Burgio, U. Lombardo, H.-J. Schulze, and W. Zuo, Phys. Rev. C **69**, 018801 (2004).
[39] R. C. Allen *et al*., Phys. Rev. D **47**, 11 (1993).
[40] D. A. Krakauer *et al*., Phys. Lett. **B252**, 177 (1990).
[41] E. E. Kolomeitsev and D. N. Voskresensky, Phys. Rev. C **68**, 015803 (2003).
[42] R. Knorren, M. Prakash, and P. J. Ellis, Phys. Rev. C **52**, 3470 (1995).
[43] M. Baldo, G. F. Burgio, and H.-J. Schulze, Phys. Rev. C **61**, 055801 (2000).
[44] I. Vidana, A. Polls, A. Ramos, M. Hjorth-Jensen, and V. G. J. Stoks, Phys. Rev. C **61**, 025802 (2000).
[45] J. K. Bunta and S. Gmuca, Phys. Rev. C **70**, 054309 (2004).
[46] W. Zuo, A. Li, Z. H. Li, and U. Lombardo, Phys. Rev. C **70**, 055802 (2004).
[47] S. Banik and D. Bandyopadhyay, Phys. Rev. C **66**, 065801 (2002).
[48] Guo Hua, Liu Bo, and Zhang Jianwei, Phys. Rev. C **67**, 024902 (2003).
[49] P.-G. Reinhard, Rep. Prog. Phys. **52**, 439 (1989); and references therein.
[50] P. Ring, Prog. Part. Nucl. Phys. **37**, 193 (1996); and references therein.
[51] B. D. Serot and J. D. Walecka, Int. J. Mod. Phys. E **6**, 515 (1997); and references therein.
[52] G. Shen, J. Li, G. C. Hillhouse, and J. Meng, Phys. Rev. C **71**, 015802 (2005).